ACS OMEGA

http://pubs.acs.org/journal/acsodf

Article

Facile Synthesis of Carbon Dots from Amido Black 10b for Sensing in Real Samples

Jin Li,[▽] Xiaoyan Wang,[▽] Jianxin Yu, Hanqin Wang, and Xiaobo Wang*

Cite This: *ACS Omega* 2022, 7, 47002−47008

Read Online

ACCESS | Metrics & More | Article Recommendations | Supporting Information

ABSTRACT: Herein, a one-step hydrothermal synthesis method was adopted to fabricate carbon dots (CDs) from amido black 10b in a sodium hydroxide solution. The morphology and composition of the CDs were investigated by XRD, FTIR TEM, XPS, UV−vis, and fluorescence spectroscopy. The obtained CDs (AB-CDs) with an average diameter of 19.4 nm displayed a well-dispersed characteristic in aqueous solutions. The as-prepared CDs showed bright blue fluorescence and good photostability, with a high quantum yield of 24.1%. AB-CDs displayed a selective and noticeable turn-off response to Fe^{3+}. Accordingly, the quantitative detection of Fe^{3+} was achieved in the range of 5−200 μmol L^{-1} with a detection limit of 1.84 μmol L^{-1}. The fluorescence response mechanism of Fe^{3+} to AB-CDs was ascribed to static quenching due to the emergence of the ground-state complex. Moreover, ascorbic acid could restore the fluorescence of AB-CDs quenched by Fe^{3+} by reducing Fe^{3+} to Fe^{2+}. The developed nanoprobe was used to detect ascorbic acid with a limit of detection of 7.26 μmol L^{-1} in the range of 20−300 μmol L^{-1}. Furthermore, the developed sensing system was successfully applied for an Fe^{3+} assay in a lake water sample and ascorbic acid detection in a human urine sample. The AB-CD-based analytical system showed its latent practical value in the chemical analysis and bioanalytical fields.

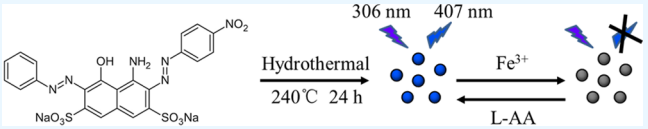

1. INTRODUCTION

Carbon dots (CDs), as a new type of fluorescent carbon nanomaterial, were first discovered inadvertently by Xu et al. in 2004.[1] Owing to their excellent physicochemical properties, such as low cost, favorable water solubility, desirable biocompatibility,[2−4] and good photostability,[5−7] they have numerous potential applications, including bioimaging,[8−11] biochemical sensors,[12−15] and nanomedicine.[16−18] Until now, the majority of recorded CDs were in the size of range below 10 nm. Only a handful of fluorescent carbon nanoparticles with diameters larger than 10 nm were reported. For example, soy milk-,[19] polyacrylamide-,[20] orange juice-,[21] and cocoon silk-derived carbon dots[22] have been successfully prepared and applied in electrocatalysis, bioimaging, and rapid cellular endocytosis. Ferric ion is one of the most common metal elements. It plays important roles in both industry and human health. Fe^{3+} is involved in diverse biochemical processes, for example, the transport and storage of oxygen and electron transfer in mitochondrial energy metabolism, and also participates in many enzymatic reactions as cofactor and improves immune function.[23] We obtain iron from foods rich in iron such as beef, egg yolks, fish, and kelp. Aberrant metabolism of Fe^{3+} will lead to a series of severe diseases. A lack of iron will lead to anemia, impaired intellectual development, reduced ability to prevent infection, and allotriophagy. In contrast, excessive iron can result in hemochromatosis, diabetes, cardiomyopathy, arrhythmia, and cancer.[24] Nowadays, water pollution is becoming more and more serious due to the arbitrary discharge of acidic industrial wastewater rich in heavy metal ions, including iron ions. Thus, it is crucial to develop suitable methods for the detection of Fe^{3+} in environmental water samples.

Amido black 10b, which contains two sulfonic acid groups and several nitrogen and oxygen atoms, is mainly used as a protein-staining reagent for polyacrylamide gel, agarose gel, and the nitrocellulose membrane. The chemical properties of amido black 10b endow it with the ability to coordinate metal ions. Ma et al. synthesized amido black 10b-stabilized silver nanoclusters and applied them for Cu^{2+} detection.[25] Yu and co-workers prepared silver nanoparticles from amido black 10b as sensors for a Cr^{3+} assay.[26] As far as we know, there is no report about the fabrication and application of carbon dots originating from amido black 10b. The heterocyclic azo chemical structure with the reactive groups of sulfonic acid, hydroxyl, and amidogen in amido black 10b may be the ideal precursor for preparing CDs.

Herein, we fabricate CDs via the one-step hydrothermal treatment of amido black 10b with the addition of NaOH (Scheme 1). The resulting CDs (AB-CDs) displayed bright blue fluorescence with a high quantum yield. Owing to their excellent fluorescence stability and the selective fluorescence response toward Fe^{3+}, AB-CDs were successfully used as

Received: September 22, 2022
Accepted: November 24, 2022
Published: December 7, 2022

https://doi.org/10.1021/acsomega.2c06047
ACS Omega 2022, 7, 47002−47008

Scheme 1. Schematic Illustration of the Fabrication of AB-CDs and Their Application for Fe^{3+} and Ascorbic Acid Assays

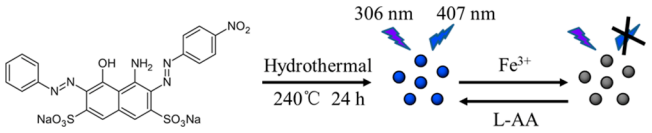

nanoprobes for the detection of Fe^{3+} at pH 5.0, with a detection limit of 1.84 μmol L^{-1}. Moreover, based on the reduction of Fe^{3+} to Fe^{2+} by ascorbic acid, the quenched fluorescence of AB-CDs by Fe^{3+} could be recovered in the presence of ascorbic acid. Thus, a selective detection system for the quantification of ascorbic acid with a detection limit of 7.26 μmol L^{-1} in the linear range of 20−300 μmol L^{-1} was established. Furthermore, the practical applicability of AB-CDs for Fe^{3+} measurements in urban lake water and ascorbic acid detection in human urine samples was verified.

2. EXPERIMENTATION

2.1. Reagents and Materials. Amido black 10b, $FeCl_3$, NaCl, KCl, $CaCl_2$, $CuCl_2$, $MgCl_2$, $FeCl_2$, $MnCl_2$, $BaCl_2$, $AlCl_3$, $CoCl_2$, $NiSO_4$, $Cr_2(SO_3)_3$, $CdSO_4$, $Zn(NO_3)_2$, $Pb(NO_3)_2$, $Hg(NO_3)_2$, sodium hydroxide, and quinine sulfate were obtained from Sinopharm Chemical Reagent Co. Ltd. Sephadex G-25 was obtained from GE Healthcare. Other reagents were used without further purification. Milli-Q-purified ultrapure water was used throughout the experiments.

2.2. Apparatuses and Characterization. High-resolution TEM (HRTEM) images were captured on a FEI Technai G2 F20 transmission electron microscope. Fourier transform infrared (FTIR) spectroscopy was performed using a Nicolet 5700 FTIR spectrometer with solid KBr pellets. X-ray photoelectron spectroscopy (XPS) measurements were performed using a Thermo (EscaLab 250Xi) X-ray photoelectron spectrometer. UV−visible absorption spectra were obtained using a Shimadzu UV−visible spectrophotometer (UV-2700). The fluorescence spectrum was recorded using Horiba fluorescence spectrometer (Fluoro Max-4). The fluorescence decay time was recorded with a FLS 980 (Edinburgh Instruments).

2.3. Synthesis of AB-CDs. 0.25 g of amido black 10b was dissolved in 10 mL of 1 M sodium hydroxide. The mixture was then transferred to a 50 mL Teflon-lined autoclave and heated at 240 °C for 24 h. After a hydrothermal treatment, the dark blue solution changed to a light brown color. The resulting product was then filtered through a 0.22 μm syringe filter, followed by gel filtration purification on Sephadex G-25. Milli-Q-purified water was adopted as an eluant. The fluorescent liquid effluent was gathered and lyophilized. The obtained powder was stored in a refrigerator at 4 °C.

2.4. Detection of Fe^{3+} and Ascorbic Acid Using AB-CDs. For the fluorescence detection of Fe^{3+}, 3 μL of an aqueous solution of AB-CDs (20 mg mL^{-1}) was added to 997 μL of a PBS solution (10 mmol L^{-1}, pH 5.0), and the solution was mixed thoroughly. Subsequently, the above solution was titrated with different mounts of Fe^{3+} (0−200 μmol L^{-1}). All samples were carefully mixed, then equilibrated for 15 min room temperature before the fluorescence measurements were performed. The fluorescence emission spectra were obtained in the wavelength range from 315 to 600 nm by exciting the sample at 306 nm. All assays were carried out in triplicate.

Ascorbic acid was tested in a PBS solution (10 mmol L^{-1}, pH 5.0) using the following steps. AB-CDs (60 μg mL^{-1}) and Fe^{3+} (750 μmol L^{-1}) were mixed in a PBS solution (10 mmol L^{-1}, pH 5.0), and the solution was incubated for 15 min at room temperature. Then, the mixture of AB-CDs and Fe^{3+} was titrated with ascorbic acid (0−300 μmol L^{-1}). All samples were mixed thoroughly and incubated for 35 min at room temperature before the assay was performed. The fluorescence emission spectra were recorded in the range from 315 to 600 nm by exciting the sample at 306 nm. All tests were run in triplicate.

2.5. Detection of Fe^{3+} and Ascorbic Acid in Real Samples. The feasibility of AB-CDs for measuring Fe^{3+} in real samples was determined in an urban lake water sample. The sample was collected from Baiyun Lake in Suizhou, China, filtered through a 0.22 μm syringe filter, and then centrifuged for 30 min at 10000 rpm. The obtained supernatant was used to prepare the Fe^{3+} solution.

The real application AB-CDs for the detection of ascorbic acid was investigated in human urine samples. The urine samples were diluted 100-fold in a PBS solution (10 mmol L^{-1}, pH 5.0) before the assay.

3. RESULTS AND DISCUSSION

3.1. Characterization of AB-CDs. The morphology of the AB-CDs was characterized by TEM, as shown in Figure 1a. According to the statistical result of one hundred particles from the TEM image, the as-prepared AB-CDs exhibited an average diameter of 19.4 nm in the range of 9.0−29.2 nm (Figure 1b). The HRTEM image (inset of Figure 1a) shows a crystalline structure with a lattice spacing of 0.218 nm, which corresponds to the (100) plane of graphitic carbon.[27,28]

3.2. Optical Properties of AB-CDs. The UV−vis absorption and fluorescence spectra of AB-CDs are displayed in Figure 2a. The aqueous solution of AB-CDs displayed two

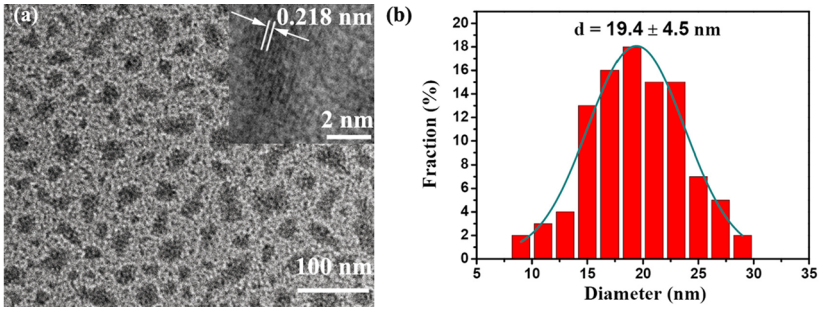

Figure 1. (a) TEM and HRTEM (inset) images of AB-CDs. (b) Particle size distribution of AB-CDs.

https://doi.org/10.1021/acsomega.2c06047
ACS Omega 2022, 7, 47002−47008

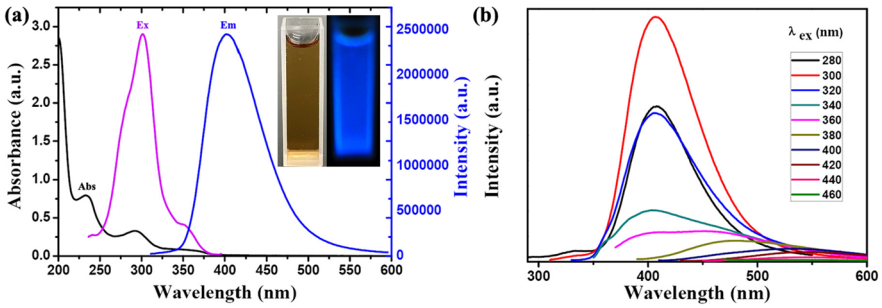

Figure 2. (a) UV−vis absorption and fluorescence spectra of AB-CDs. The inset shows photos of an AB-CD aqueous solution under sunlight (left) and UV lamp excitation (right) at 254 nm. (b) Excitation-dependent fluorescence emission spectra of AB-CDs.

obvious absorption peaks at 232 and 292 nm, which are attributed to the $\pi-\pi^*$ transitions of C═C.[29,30] Fluorescence excitation and emission spectra showed that the maximum emission intensity emerged at 407 nm when the sample was excited at 306 nm. The excitation-dependent fluorescence emission behavior of the AB-CDs is illustrated in Figure 2b. The fluorescence emission peak of the AB-CDs shifted from 404 to 545 nm when the excitation wavelength was changed from 340 to 460 nm. The fluorescence quantum yield of the aqueous solution of AB-CDs was calculated to be 24.1% using quinine sulfate (QY = 0.54) as the reference.[31]

FTIR and XPS investigations were used to identify the characteristic functional groups of the AB-CDs. As displayed in Figure S1, the absorption peak at 1132 cm^{-1} belonged to the stretching vibration of C−O,[32] and the band at 3437 cm^{-1} belonged to C−OH.[33] The band at 1369 cm^{-1} was attributed to the stretching vibration of C−N. The bands at 1626 and 1666 cm^{-1} were ascribed to stretching vibrations of C═C. The band at 1927 cm^{-1} was ascribed to the stretching vibration of C−C. The peak at 2552 cm^{-1} was attributed to the stretching vibration of S−H.[34] The band at 2924 cm^{-1} was ascribed to the stretching vibration of C−H.

The full XPS spectrum is illustrated in Figure 3a. The peaks at 169.1, 284.7, and 531.6 eV were attributed to S 2p, C 1s, and O 1s, respectively. The peaks centered at 1071.2 and 497.1 eV correspond to Na^+ signals.[35−37] A very weak peak at 399.8 eV corresponding to N 1s was almost invisible (Figure S2), indicating the extremely low N doping, which was further proved by the element proportion analysis of the AB-CDs from the XPS results (Table S1). The high-resolution S 2p, C 1s, and O 1s spectra are shown in Figure 3b−d, respectively. Two fitted peaks at 168.5 and 169.5 eV in the S 2p spectrum could be attributed to C−SO_x (x = 2, 3) groups, indicating the presence of oxidized S on the surface of the AB-CDs.[38] The C 1s spectrum showed three peaks at 284.6, 285.9, and 289.9 eV corresponding to C−C or C═C, C−O, and O−C═O moieties, respectively.[39−41] The O 1s spectrum displayed three peaks at 531.3, 532.5, and 535.6 eV, representing the C═O and C−O bonds and the adsorption of surface water, respectively.[42−44] Both the FTIR and XPS results affirmed that sulfur functional groups and hydroxyl moieties exist on the exterior of the AB-CDs.

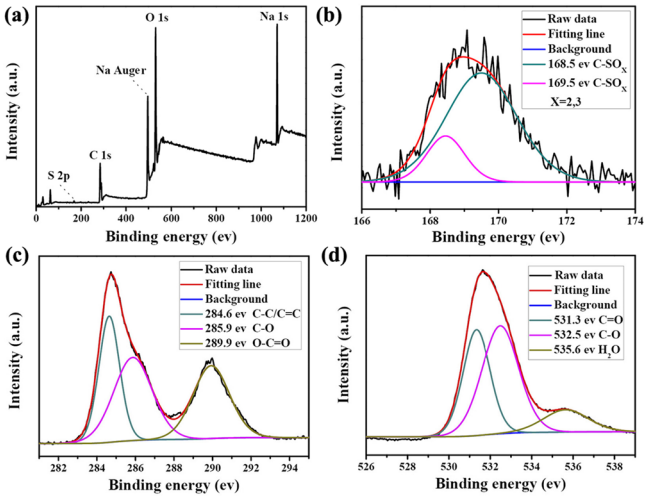

Figure 3. (a) Full XPS survey spectrum of AB-CDs. (b) XPS S 2p results. (c) XPS C 1s results. (d) XPS O 1s results of the prepared AB-CDs.

3.3. Stability of AB-CDs. The fluorescence stability of AB-CDs toward different ionic strengths, pH values, and extended UV exposure was investigated, and the results are displayed in Figure 4. The emission intensity of the AB-CDs decreased slightly upon the addition of NaCl solutions of various concentrations (0.1−1.0 mol L^{-1}) (Figure 4a). AB-CDs exhibited excellent photostability within the wide pH range of 3−12 (Figure 4b). The fluorescence intensity of the AB-CDs declined slightly even after 1 h of exposure to UV light (Figure 4c). These superior properties would allow AB-CDs to be a latent candidate for sensing application in real samples.

3.4. Detection of Fe^{3+} and Ascorbic Acid Using AB-CDs. In order to get the ideal results for the Fe^{3+} and ascorbic acid assays, the effect of the pH value of PBS, the concentration of AB-CDs, the concentration of Fe^{3+}, the reaction time of Fe^{3+}, and the reaction time of ascorbic acid were investigated and optimized. The equation below shows the fluorescence quenching efficiency of AB-CDs by Fe^{3+} and the fluorescence recovering capacity of ascorbic acid in PBS solution.

$$\mathrm{Eff_q}(\%) = (F_0 - F)/F_0$$
$$\mathrm{Eff_r}(\%) = (F_r - F)/(F_0 - F) \quad (1)$$

Here F_0 and F indicate the emission intensities of AB-CDs at 407 nm in the absence and presence of Fe^{3+}. F_r represents the restored fluorescence intensity of AB-CDs at 407 nm after the addition of ascorbic acid. As illustrated in Figure S3a, $\mathrm{Eff_q}$ decreased progressively as the pH increased from 3.0 to 7.0; $\mathrm{Eff_r}$ increased slowly as the pH increased from 3.0 to 5.0, then decreased as the pH increased from 5.0 to 7.0. Thus, pH 5.0 was selected as the optimal pH for subsequent experiments. As shown in Figure S3b, $\mathrm{Eff_q}$ decreased gradually when the concentration of AB-CDs changed from 20 to 150 $\mu g\ mL^{-1}$;

https://doi.org/10.1021/acsomega.2c06047
ACS Omega 2022, 7, 47002−47008

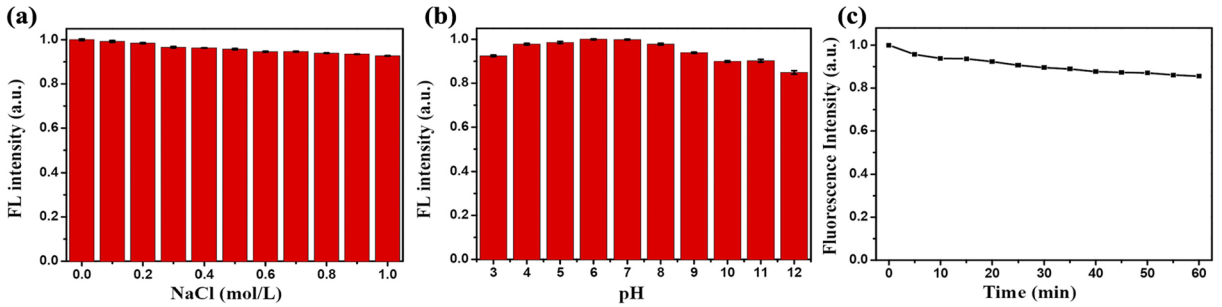

Figure 4. (a) Effect of various ionic strengths on the fluorescence emission intensity of AB-CDs. (b) Influence of pH values on the fluorescence intensity of AB-CDs. (c) Influence of extended UV exposure on the fluorescence intensity of AB-CDs.

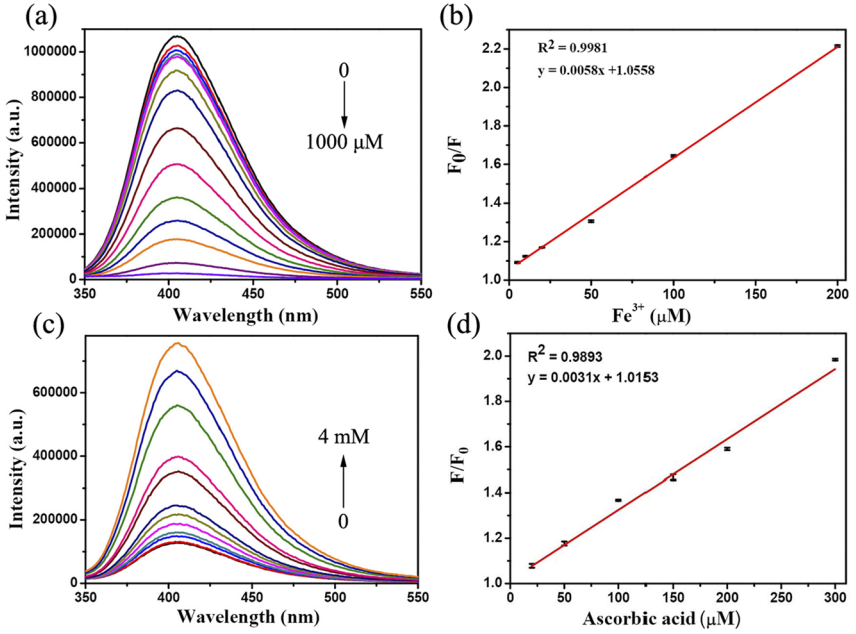

Figure 5. (a) Fluorescence emission spectra of AB-CDs (60 μg mL^{-1} in a 10 mmol L^{-1} PBS solution, pH 5.0) after the addition of Fe^{3+} (0−1000 μmol L^{-1}). F and F_0 are the fluorescence emission intensities of AB-CDs at 407 nm (excitation wavelength of 306 nm) in the presence and absence of Fe^{3+}, respectively. (b) Linear relation between F_0/F and the concentration of Fe^{3+} (from left to right: 5, 10, 20, 50, 100, and 200 μmol L^{-1}). (c) Fluorescence response of the AB-CDs/Fe^{3+} detection system upon the addition of ascorbic acid (0−4 mmol L^{-1}) in a 10 mmol L^{-1} PBS solution (pH 5.0). (d) Relationship between F_0/F and the concentration of ascorbic acid (from left to right: 20, 50, 100, 150, 200, and 300 μmol L^{-1}).

Eff_r increased stepwise as the concentration of AB-CDs increased from 20 to 60 μg mL^{-1}, then decreased slowly as the concentration increased from 60 to 150 μg mL^{-1}. Thus, 60 μg mL^{-1} was set as the probe concentration. Figure S3c show that the most suitable concentration of Fe^{3+} was 750 μmol L^{-1} for the ascorbic acid assay. Figure S3d shows that a remarkable fluorescence quenching response of AB-CDs (60 μg mL^{-1}) toward Fe^{3+} (750 μmol L^{-1}) was observed within about 1 min, then the fluorescence emission intensity of AB-CDs remained relatively stable between 15 min and 1 h. Hence, 15 min was selected as the incubation time for the Fe^{3+} assay. The emission intensity of the admixture of AB-CDs/Fe^{3+} increased gradually and peaked at 35 min after the addition of ascorbic acid (Figure S3e). Thus, 35 min was selected as the incubation time for ascorbic acid detection.

Under these optimal conditions, the fluorescence response of AB-CDs toward various amounts of Fe^{3+} (5−200 μmol L^{-1}) in a PBS solution (pH 5.0) were investigated.

As displayed in Figure 5a, the fluorescence emission intensity of AB-CDs at 407 nm declined gradually with the increase in the concentration of Fe^{3+}. Figure 5b depicts the plot of F_0/F versus the concentration of Fe^{3+}. The ratio of F_0/F displayed a good linear relationship (R^2 = 0.9981) with the concentration of Fe^{3+} in the range of 20−300 μmol L^{-1}, where F and F_0 represent the fluorescence intensities of AB-CDs at 407 nm in the presence and absence of Fe^{3+}, respectively. The limit of detection was calculated to be 1.84 μmol L^{-1} (based on the equation of $3\sigma/k$, where σ denotes the standard deviation of the blank measurement and k represents the slope of the linear calibration graph), which was comparable to the data reported previously for other carbon dot-based probes for Fe^{3+} detection in environmental water samples (Table S2).

To investigate the selective response of AB-CDs toward Fe^{3+}, different metal ions (500 μmol L^{-1}) were mixed with CDs (60 μg mL^{-1}) in a PBS solution (pH 5.0). After 15 min of incubation at room temperature, the fluorescence spectra in the wavelength range of 315−600 nm were collected under excitation at 306 nm. As depicted in Figure S4, AB-CDs exhibited a distinct selectivity for Fe^{3+} over other metal ions in a 10 mmol L^{-1} PBS solution (pH 5.0), suggesting their potential use for an Fe^{3+} assay.

https://doi.org/10.1021/acsomega.2c06047
ACS Omega 2022, 7, 47002−47008

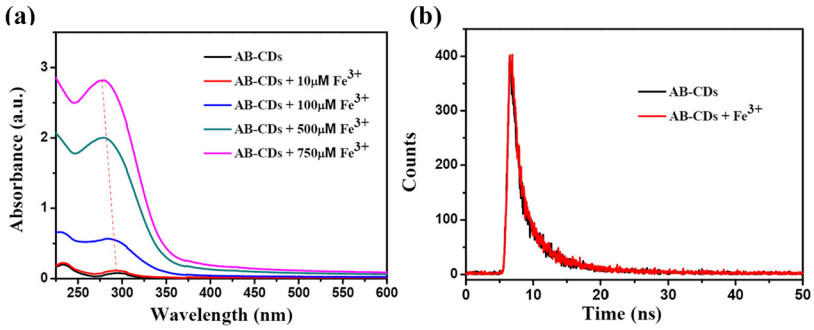

Figure 6. (a) UV−vis spectra of AB-CDs (60 μg mL^{-1} in a 10 mmol L^{-1} PBS solution, pH 5.0) before and after the addition of Fe^{3+} (10−750 μmol L^{-1}). (b) Fluorescence decay spectra of AB-CDs (60 μg mL^{-1}, black curve; after the addition of 750 μmol L^{-1} Fe^{3+}, red curve) at excitation and emission wavelengths of 306 and 407 nm, respectively.

Fe^{3+} could be converted into Fe^{2+} by ascorbic acid based on the oxidation−reduction reaction. As anticipated, ascorbic acid could restore the quenched fluorescence of the AB-CDs/Fe^{3+} complex (Figure S5). Figure 5c shows that the fluorescence intensity of the AB-CDs/Fe^{3+} complex were gradually increased after the addition of ascorbic acid. The ratio of F_0/F displayed a favorable linear relationship (Figure 5d, R^2 = 0.9893) with the concentration of ascorbic acid in the range of 20−300 μmol L^{-1}, where F and F_0 represent the fluorescence intensities of AB-CDs at 407 nm in the presence and absence of ascorbic acid, respectively. The limit of detection was calculated to be 7.26 μmol L^{-1} (based on the equation $3\sigma/k$), which was comparable to the data reported previously for other carbon dot-based probes (Table S3).

We further investigated the selectivity of the AB-CDs/Fe^{3+} complex for the detection of ascorbic acid. Various cations (Na^+, K^+, Ca^{2+}, and Mg^{2+}), glutathione, and amino acids (glycine, serine, glutamic acid, histidine, theronine, and L-cysteine) were added into the mixture of AB-CDs/Fe^{3+}. The concentration of ascorbic acid and each interference was 500 μmol L^{-1}. Figure S6 shows that the fluorescence intensities of the AB-CDs/Fe^{3+} complex increased significantly in the presence of ascorbic acid. Most interferents had unconspicuous effects on the fluorescence intensity of AB-CDs/Fe^{3+}. The result reflected excellent ability of AB-CDs/Fe^{3+} to selectively test for ascorbic acid.

3.5. Potential Mechanism of Fluorescence Response of AB-CDs toward Fe^{3+}. In most cases, the fluorescence quenching mechanism of CDs by a quencher arises from dynamic quenching, static quenching, inner filter effect (IFE), Förster resonance energy transfer (FRET), or PET (photo-induced electron transfer).To investigate the latent mechanism of fluorescence quenching of AB-CDs by Fe^{3+}, UV−vis absorbance spectroscopy, fluorescence spectroscopy, Stern−Volmer equation analysis, and a fluorescence lifetime assay were carried out.

When static quenching occurs, the specific absorbance apex of the carbon dots will shift to a longer or shorter wavelength in the presence of the quencher. As depicted in Figure 6a, the absorbance intensity increased with the Fe^{3+} content. The characteristic absorption band at 294 nm shifted to 280 nm (red dash line in Figure 6a) upon the addition of Fe^{3+} (750 μmol L^{-1}), which probably originates from the coordinating of Fe^{3+} and the reactive moieties on the exterior of AB-CDs, indicating the emergence of the ground-state complex originates from the static quenching mechanism of AB-CDs.

As shown in Figure 5a, neither fluorescence shifts nor new emission peaks were observed in the fluorescence spectra of AB-CDs in the presence of Fe^{3+}, implying that the quenching of AB-CDs by Fe^{3+} is not attributed to FRET.

The Stern−Volmer equation is the conventional method of distinguishing the mechanisms of static quenching and dynamic quenching. When static quenching emerges, it follows the equation below:

$$F_0/F = 1 + K_{sv}[Q] \quad (2)$$

Dynamic quenching abides by the following similar equation:

$$F_0/F = \tau_0/\tau = 1 + K[Q] \quad (3)$$

where F_0 is the fluorescence intensity of the AB-CDs, F is the fluorescence intensity of the AB-CDs after the addition of Fe^{3+}, K_{sv} denotes the static quenching constant of the Stern−Volmer equation, τ_0 and τ are the fluorescent lifetime in the absence and presence of the quencher, respectively, and K represents the formation constant of the fluorophore and the quencher.

The Stern−Volmer equation of AB-CDs toward Fe^{3+} was analyzed. The quenching process AB-CDs toward Fe^{3+} abided by the following Stern−Volmer equation: $F_0/F = 1 + K_{sv}[Q]$. It displayed a linear relationship, with $K_{sv} = 5.8 \times 10^3$ mol L^{-1}.

Fluorescence lifetime analysis is the most accurate technique to differentiate the mechanisms of static quenching, dynamic quenching, FRET, and PET. Under the circumstance of static quenching, the addition of the quencher does not alter the fluorescent lifetime of CDs ($\tau_0/\tau = 1$). However, the addition a quencher will reduce the fluorescence lifetime of CDs over the course of dynamic quenching. As illustrated in Figure 6b, the average fluorescence lifetime of AB-CDs remained nearly constant from 3.65 to 3.62 ns in the absence and presence of Fe^{3+} (Table S4). Hence, the feasibility of dynamic quenching, FRET, and PET can be eliminated because there is no obvious change of the fluorescence lifetime in the quenching process.

It should be noted that the absorbance spectra of Fe^{3+} and the excitation and emission spectra of AB-CDs partially coincide (Figure S7), implying that the fluorescence quenching of AB-CDs by Fe^{3+} may be partly ascribed to IFE. Usually, IFE is inescapable over the course of quenching in each fluorescence measurement because of the reduction of the excitation beam or the absorption of emitted radiation by the large amount of AB-CDs or Fe^{3+} in solution.

The relatively large magnitude of the quenching constant (K_{sv}) and the relatively unchanged fluorescence lifetime

https://doi.org/10.1021/acsomega.2c06047
ACS Omega 2022, 7, 47002−47008

indicate that the quenching of AB-CDs by Fe^{3+} may be attributed to static quenching.[45−47]

3.6. Detection of Fe^{3+} and Ascorbic Acid in Real Samples. The real application of AB-CDs for an Fe^{3+} assay in an urban lake water sample was investigated. As illustrated in Table S5, the relative standard deviation (less than 0.91%, n = 3) and the recoveries (90.4%−113.7%) were acceptable.

The feasibility of using the mixture of AB-CDs and Fe^{3+} to detect ascorbic acid was investigated in a human urine sample. As depicted in Table S6, the relative standard deviation (less than 0.95%, n = 3) and the recoveries (91.5%−115.3%) were agreeable. The results confirmed the credibility of the AB-CDs/Fe^{3+} sensing platform for ascorbic acid detection in real samples.

4. CONCLUSIONS

AB-CDs were prepared from amido black 10b in a sodium hydroxide solution via a single-step hydrothermal strategy. The prepared AB-CDs showed excellent fluorescence properties with a high quantum yield. Based on the selective and sensitive response of Fe^{3+} by AB-CDs, the synthesized AB-CDs were successfully applied for Fe^{3+} detection in a lake water sample. Furthermore, the fluorescence of AB-CDs quenched by Fe^{3+} could be restored in the presence of ascorbic acid. Thus, the AB-CDs/Fe^{3+} sensing system was applied to detect ascorbic acid in a real urine sample. The AB-CD-based nanoprobe displayed its latent practical value for the chemical analysis and bioanalytical fields because of its easy fabrication, convenient operation, and low cost.

■ ASSOCIATED CONTENT

Supporting Information

The Supporting Information is available free of charge at https://pubs.acs.org/doi/10.1021/acsomega.2c06047.

FTIR spectrum of AB-CDs; magnified N 1s region of the XPS wide-survey spectrum of AB-CDs; element content analysis of AB-CDs; influence of the pH value of PBS, the concentration of AB-CDs, the concentration of Fe^{3+}, and the reaction time of the AB-CD-based sensing platform on the determination of Fe^{3+} and ascorbic acid; selectivity of AB-CDs upon various metal ions; comparison of AB-CDs and other carbon dot-based probes for Fe^{3+} and ascorbic acid detection; images of AB-CDs in the presence of Fe^{3+} and ascorbic acid; selectivity of AB-CDs/Fe^{3+} platform upon ascorbic acid; double-exponential fitting of AB-CDs and AB-CDs/Fe^{3+} decay curves; Fe^{3+} determination results in urban lake water samples; and ascorbic acid detection results in a human urine sample (PDF)

■ AUTHOR INFORMATION

Corresponding Author

Xiaobo Wang − *Reproductive Medicine Center, Suizhou Hospital and Center for Translational Medicine, Suizhou Hospital, Hubei University of Medicine, Suizhou, Hubei 441300, People's Republic of China;* orcid.org/0000-0001-8791-470X; Email: xbwang@hbmu.edu.cn

Authors

Jin Li − *Reproductive Medicine Center, Suizhou Hospital, Hubei University of Medicine, Suizhou, Hubei 441300, People's Republic of China*

Xiaoyan Wang − *Reproductive Medicine Center, Suizhou Hospital, Hubei University of Medicine, Suizhou, Hubei 441300, People's Republic of China*

Jianxin Yu − *Center for Translational Medicine, Suizhou Hospital, Hubei University of Medicine, Suizhou, Hubei 441300, People's Republic of China*

Hanqin Wang − *Center for Translational Medicine, Suizhou Hospital, Hubei University of Medicine, Suizhou, Hubei 441300, People's Republic of China*

Complete contact information is available at: https://pubs.acs.org/10.1021/acsomega.2c06047

Author Contributions

[▽]These authors contributed equally to this work. Jin Li and Xiaoyan Wang participated in the main part of the research, Jianxin Yu and Hanqin Wang assisted in the data analysis, and Xiaobo Wang wrote manuscript for publication.

Notes

The authors declare no competing financial interest.

All experimentations were carried out in accordance with the ethics standards of Suizhou Central Hospital, Hubei University of Medicine.

■ ACKNOWLEDGMENTS

This work was supported by the Advantages Discipline Group (Medicine) Project in Higher Education of Hubei Province (2021-2025, 2022XKQY7), the Natural Science Foundation of Hubei Province of China (2018CFC869), the Natural Science Foundation of of Hubei Provincial Department of Education (B2018112, Q20132102), the Foundation for Fostering the National Natural Science Foundation of Hubei University of Medicine (2013GPY02), the Initial Project for Post-Graduates of Hubei University of Medicine (2011QDZR-4).

■ REFERENCES

(1) Xu, X.; Ray, R.; Gu, Y.; Ploehn, H. J.; Gearheart, L.; Raker, K.; Scrivens, W. A. Electrophoretic analysis and purification of fluorescent single-walled carbon nanotube fragments. *J. Am. Chem. Soc.* **2004**, *126*, 12736−12737.

(2) Cui, F.; Sun, J.; Ji, J.; Yang, X.; Wei, K.; Xu, H.; Gu, Q.; Zhang, Y.; Sun, X. Carbon dots-releasing hydrogels with antibacterial activity, high biocompatibility, and fluorescence performance as candidate materials for wound healing. *J. Hazard. Mater.* **2021**, *406*, 124330.

(3) Wareing, T. C.; Gentile, P.; Phan, A. N. Biomass-Based Carbon Dots: Current Development and Future Perspectives. *ACS Nano* **2021**, *15*, 15471−15501.

(4) Ge, G.; Li, L.; Wang, D.; Chen, M.; Zeng, Z.; Xiong, W.; Wu, X.; Guo, C. Carbon dots: synthesis, properties and biomedical applications. *J. Mater. Chem. B* **2021**, *9*, 6553−6575.

(5) Boakye-Yiadom, K. O.; Kesse, S.; Opoku-Damoah, Y.; Filli, M. S.; Aquib, M.; Joelle, M. M. B.; Farooq, M. A.; Mavlyanova, R.; Raza, F.; Bavi, R.; et al. Carbon dots: Applications in bioimaging and theranostics. *Int. J. Pharm.* **2019**, *564*, 308−317.

(6) Liu, H.; Guo, J.; Aryee, A. A.; Hua, L.; Sun, Y.; Li, Z.; Liu, J.; Tang, W. Lighting up individual organelles with fluorescent carbon dots. *Front. Chem.* **2021**, *9*, 784851.

(7) Mutuyimana, F. P.; Liu, J.; Nsanzamahoro, S.; Na, M.; Chen, H.; Chen, X. Yellow-emissive carbon dots as a fluorescent probe for chromium (VI). *Microchim. Acta* **2019**, *186*, 163.

(8) Du, J.; Xu, N.; Fan, J.; Sun, W.; Peng, X. Carbon dots for in vivo bioimaging and theranostics. *Small* **2019**, *15*, 1805087.

(9) Ansari, L.; Hallaj, S.; Hallaj, T.; Amjadi, M. Doped-carbon dots: Recent advances in their biosensing, bioimaging and therapy applications. *Colloids Surf., B* **2021**, *203*, 111743.

(10) Karakoçak, B. B. m.; Laradji, A.; Primeau, T.; Berezin, M. Y.; Li, S.; Ravi, N. Hyaluronan-conjugated carbon quantum dots for bioimaging use. *ACS Appl. Mater. Interfaces* **2021**, *13*, 277−286.
(11) Kailasa, S. K.; Koduru, J. R. Perspectives of magnetic nature carbon dots in analytical chemistry: From separation to detection and bioimaging. *Trends Environ. Anal. Chem.* **2022**, *33*, No. e00153.
(12) Fan, Q.; Li, J.; Zhu, Y.; Yang, Z.; Shen, T.; Guo, Y.; Wang, L.; Mei, T.; Wang, J.; Wang, X. Functional carbon quantum dots for highly sensitive graphene transistors for Cu2+ ion detection. *ACS Appl. Mater. Interfaces* **2020**, *12*, 4797−4803.
(13) Mohandoss, S.; Khanal, H. D.; Palanisamy, S.; You, S.; Shim, J.-J.; Lee, Y. R. Multiple heteroatom-doped photoluminescent carbon dots for ratiometric detection of Hg 2+ ions in cell imaging and environmental applications. *Anal. Methods* **2022**, *14*, 635−642.
(14) Li, Z.; Zhang, J.; Sun, Q.; Shi, W.; Tao, T.; Fu, Y. Moxifloxacin detection based on fluorescence resonance energy transfer from carbon quantum dots to moxifloxacin using a ratiometric fluorescence probe. *New J. Chem.* **2022**, *46*, 4226−4232.
(15) Yusuf, V. F.; Atulbhai, S. V.; Swapna, B.; Malek, N. I.; Kailasa, S. K. Recent developments on carbon dots-based green analytical methods: New opportunities in fluorescence assay of pesticides, drugs and biomolecules. *New J. Chem.* **2022**, *46*, 14287−14308.
(16) Zhang, W.; Sigdel, G.; Mintz, K. J.; Seven, E. S.; Zhou, Y.; Wang, C.; Leblanc, R. M. Carbon dots: A future Blood−Brain Barrier penetrating nanomedicine and drug nanocarrier. *Int. J. Nanomed* **2021**, *16*, 5003−5016.
(17) Chan, K. K.; Yap, S. H. K.; Yong, K.-T. Biogreen synthesis of carbon dots for biotechnology and nanomedicine applications. *Nano-Micro Lett.* **2018**, *10*, 72.
(18) Zhang, X.; Jiang, J.; Yu, Q.; Zhou, P.; Yang, S.; Xia, J.; Deng, T.; Yu, C. ZIF-based carbon dots with lysosome-Golgi transport property as visualization platform for deep tumour therapy via hierarchical size/charge dual-transform and transcytosis. *Nanoscale* **2022**, *14*, 8510−8524.
(19) Zhu, C.; Zhai, J.; Dong, S. Bifunctional fluorescent carbon nanodots: green synthesis via soy milk and application as metal-free electrocatalysts for oxygen reduction. *Chem. Commun.* **2012**, *48*, 9367−9369.
(20) Gu, J.; Wang, W.; Zhang, Q.; Meng, Z.; Jia, X.; Xi, K. Synthesis of fluorescent carbon nanoparticles from polyacrylamide for fast cellular endocytosis. *RSC Adv.* **2013**, *3*, 15589−15591.
(21) Sahu, S.; Behera, B.; Maiti, T. K.; Mohapatra, S. Simple one-step synthesis of highly luminescent carbon dots from orange juice: application as excellent bio-imaging agents. *Chem. Commun.* **2012**, *48*, 8835−8837.
(22) Li, W.; Zhang, Z.; Kong, B.; Feng, S.; Wang, J.; Wang, L.; Yang, J.; Zhang, F.; Wu, P.; Zhao, D. Simple and green synthesis of nitrogen-doped photoluminescent carbonaceous nanospheres for bioimaging. *Angew. Chem., Int. Ed* **2013**, *52*, 8151−8155.
(23) Lynch, S. R. Interaction of iron with other nutrients. *Nutr. Rev.* **1997**, *55*, 102−110.
(24) Andrews, P. A. Disorders of iron metabolism. *N. Engl. J. Med.* **2000**, *342*, 1293−1294.
(25) Ma, F.; Liang, S.; Peng, Y.; Kuang, Y.; Zhang, X.; Chen, S.; Long, Y.; Zeng, R. Copper ion detection using novel silver nanoclusters stabilized with amido black 10B. *Anal. Bioanal. Chem.* **2016**, *408*, 3239−3246.
(26) Yu, H.; Wang, Z.; Huang, W. Highly stable and sensitive colorimetric visualization of trivalent chromium using amido black 10B-stabilized silver nanoparticles. *Plasmonics* **2018**, *13*, 1459−1465.
(27) Tian, T.; He, Y.; Ge, Y.; Song, G. One-pot synthesis of boron and nitrogen co-doped carbon dots as the fluorescence probe for dopamine based on the redox reaction between Cr (VI) and dopamine. *Sens. Actuators, B* **2017**, *240*, 1265−1271.
(28) Jia, Y.; Hu, Y.; Li, Y.; Zeng, Q.; Jiang, X.; Cheng, Z. Boron doped carbon dots as a multifunctional fluorescent probe for sorbate and vitamin B12. *Microchim. Acta* **2019**, *186*, 84.
(29) Xue, M.; Zhang, L.; Zhan, Z.; Zou, M.; Huang, Y.; Zhao, S. Sulfur and nitrogen binary doped carbon dots derived from ammonium thiocyanate for selective probing doxycycline in living cells and multicolor cell imaging. *Talanta* **2016**, *150*, 324−330.
(30) Qiao, L.; Sun, T.; Zheng, X.; Zheng, M.; Xie, Z. Exploring the optimal ratio of D-glucose/L-aspartic acid for targeting carbon dots toward brain tumor cells. *Mater. Sci. Eng., C* **2018**, *85*, 1−6.
(31) Dong, Y.; Pang, H.; Yang, H. B.; Guo, C.; Shao, J.; Chi, Y.; Li, C. M.; Yu, T. Carbon-based dots co-doped with nitrogen and sulfur for high quantum yield and excitation-independent emission. *Angew. Chem., Int. Ed* **2013**, *52*, 7800−7804.
(32) Jin, X.; Sun, X.; Chen, G.; Ding, L.; Li, Y.; Liu, Z.; Wang, Z.; Pan, W.; Hu, C.; Wang, J. pH-sensitive carbon dots for the visualization of regulation of intracellular pH inside living pathogenic fungal cells. *Carbon* **2015**, *81*, 388−395.
(33) Liu, Y.; Kim, D. Y. Ultraviolet and blue emitting graphene quantum dots synthesized from carbon nano-onions and their comparison for metal ion sensing. *Chem. Commun.* **2015**, *51*, 4176−4179.
(34) Van Tam, T.; Hong, S. H.; Choi, W. M. Facile synthesis of cysteine-functionalized graphene quantum dots for a fluorescence probe for mercury ions. *RSC Adv.* **2015**, *5*, 97598−97603.
(35) López, C.; Zougagh, M.; Algarra, M.; Rodríguez-Castellón, E.; Campos, B.; da Silva, J. C. G. E.; Jiménez-Jiménez, J.; Ríos, A. Microwave-assisted synthesis of carbon dots and its potential as analysis of four heterocyclic aromatic amines. *Talanta* **2015**, *132*, 845−850.
(36) Li, W.; Zhu, J.; Xie, G.; Ren, Y.; Zheng, Y.-Q. Ratiometric system based on graphene quantum dots and Eu3+ for selective detection of tetracyclines. *Anal. Chim. Acta* **2018**, *1022*, 131−137.
(37) Xu, X.; Tang, W.; Zhou, Y.; Bao, Z.; Su, Y.; Hu, J.; Zeng, H. Steering photoelectrons excited in carbon dots into platinum cluster catalyst for solar-driven hydrogen production. *Adv. Sci.* **2017**, *4*, 1700273.
(38) Li, F.; Sun, L.; Luo, Y.; Li, M.; Xu, Y.; Hu, G.; Li, X.; Wang, L. Effect of thiophene S on the enhanced ORR electrocatalytic performance of sulfur-doped graphene quantum dot/reduced graphene oxide nanocomposites. *RSC Adv.* **2018**, *8*, 19635−19641.
(39) Wang, N.; Wang, Y.; Guo, T.; Yang, T.; Chen, M.; Wang, J. Green preparation of carbon dots with papaya as carbon source for effective fluorescent sensing of Iron (III) and Escherichia coli. *Biosens. Bioelectron* **2016**, *85*, 68−75.
(40) Wang, C.; Xu, Z.; Cheng, H.; Lin, H.; Humphrey, M. G.; Zhang, C. A hydrothermal route to water-stable luminescent carbon dots as nanosensors for pH and temperature. *Carbon* **2015**, *82*, 87−95.
(41) Xu, Z.-Q.; Yang, L.-Y.; Fan, X.-Y.; Jin, J.-C.; Mei, J.; Peng, W.; Jiang, F.-L.; Xiao, Q.; Liu, Y. Low temperature synthesis of highly stable phosphate functionalized two color carbon nanodots and their application in cell imaging. *Carbon* **2014**, *66*, 351−360.
(42) Miao, H.; Wang, L.; Zhuo, Y.; Zhou, Z.; Yang, X. Label-free fluorimetric detection of CEA using carbon dots derived from tomato juice. *Biosens. Bioelectron* **2016**, *86*, 83−89.
(43) Zhang, T.; Zhu, J.; Zhai, Y.; Wang, H.; Bai, X.; Dong, B.; Wang, H.; Song, H. A novel mechanism for red emission carbon dots: hydrogen bond dominated molecular states emission. *Nanoscale* **2017**, *9*, 13042−13051.
(44) Mu, Y.; Wang, N.; Sun, Z.; Wang, J.; Li, J.; Yu, J. Carbogenic nanodots derived from organo-templated zeolites with modulated full-color luminescence. *Chem. Sci.* **2016**, *7*, 3564−3568.
(45) Zu, F.; Yan, F.; Bai, Z.; Xu, J.; Wang, Y.; Huang, Y.; Zhou, X. The quenching of the fluorescence of carbon dots: a review on mechanisms and applications. *Microchim. Acta* **2017**, *184*, 1899−1914.
(46) Shi, L.; Hou, Z.; Zhang, C.; Zhang, G.; Zhang, Y.; Dong, C.; Shuang, S. Concentration-dependent multicolor fluorescent carbon dots for colorimetric and fluorescent bimodal detections of Fe 3+ and l-ascorbic acid. *Anal. Methods* **2019**, *11*, 669−676.
(47) Chen, Y.; Sun, X.; Pan, W.; Yu, G.; Wang, J. Fe^{3+}-sensitive carbon dots for detection of Fe^{3+} in aqueous solution and intracellular imaging of Fe^{3+} inside fungal cells. *Front. Chem.* **2020**, *7*, 911.

https://doi.org/10.1021/acsomega.2c06047
ACS Omega 2022, 7, 47002−47008